Coded Spectral Doppler Imaging: from simulation to real-time processing

Coded Spectral Doppler Imaging: from simulation to real-time processing

Alessandro Ramalli, Enrico Boni, Alessandro Dallai, Francesco Guidi, Stefano Ricci, Piero Tortoli

***Abstract*— Transmission of coded pulses and matched receive filtering can improve the ultrasound imaging penetration depth while preserving the axial resolution. This paper shows that the pulse compression technique may be integrated in a low-cost scanner to be profitably used also in spectral Doppler investigations. By operating on beamformed, demodulated and down-sampled data in the frequency domain, a single digital signal processor is proved sufficient to perform both pulse compression and (multigate) spectral Doppler algorithms in real-time. Simulations, phantom and in vivo experiments demonstrate that the transmission of (2.5 µs or 5µs long) linear frequency modulated chirps with bandwidths over the range 1.6-5.4 MHz, rather than of corresponding sine burst pulses, provide SNR improvements very close to theory. Even in the presence of selective tissue attenuation, SNR gains up to 11dB and 13.3dB have been obtained for the short and the longer chirp, respectively. This may be important in clinical Doppler applications where the needed penetration depth is not achieved with sufficient SNR unless very long bursts are transmitted.**

***Index Terms*— real-time pulse compression; chirp signals; spectral Doppler, multigate spectral Doppler**

I. Introduction

PULSE compression is a signal processing technique, first proposed for radar applications, which requires the transmission of coded pulses and processing of the corresponding echoes through a matched filter. Several studies have discussed the advantages of this technique in ultrasound medical applications [1], [2], highlighting the possibility of achieving improved penetration depth [3] and better axial resolution [4] without increasing the mechanical index.

Unfortunately, the high computational cost, especially when associated to the use of array probes, have for long time limited the massive real-time application of pulse compression. Most implementation efforts were so far directed toward fundamental [3], [5]–[7], harmonic and contrast [8]–[14], as well as elastography [15]–[17] imaging applications. However, also the quality of Doppler ultrasound blood flow investigations is often hampered by a low signal to noise ratio (SNR), especially in deep vessels. This problem, for example, may be met during transcranial Doppler exams in elder subjects, investigations of the stenotic internal carotid arteries in burly patients [18], or in cardiac applications. Even though the coded transmission can represent an ideal tool to improve the SNR, only in a few cases it was actually used for blood flow investigations (see, e.g. [19]–[22]) and, at the best of our knowledge, no results of real-time application to spectral Doppler were presented so far in the literature. The availability of coded transmission and pulse compression is advertised in the description of some commercial systems like the iU22 by Philips Healthcare (Amsterdam, The Netherlands) and the ACUSON Sequoia 512 by Siemens Healthcare (Erlangen, Germany), for color Doppler imaging, but no information is given about the related implementation.

This paper reports a detailed description of the hardware and software developed to perform pulse compression in real-time spectral Doppler investigations. In particular, it is shown that such implementation is feasible in a low-cost open scanner by suitably coding one single-core digital signal processor (DSP). The firmware and software of the ULA-OP [23] were in fact adapted to transmit chirp signals with arbitrary tapering window and to compress the echo signals in a matched filter. The latter operation, in particular, is performed in the frequency domain, by multiplying the spectrum of the received echo-signal by suitable coefficients, and transforming the product back to the time domain. The computation is so efficient that the subsequent spectral Doppler analysis is not limited to a single sample volume, but can be extended to multiple sample volumes according to the so called multigate spectral Doppler (MSD) method [24].

Preliminary results of this approach were presented in [25]. In this paper, the proposed pulse compression method for spectral Doppler imaging is thoroughly investigated by means of simulations, phantom and in vivo experiments. These were carried out to evaluate the performance, in terms of SNR and axial resolution, attainable by chirp signals with different time-bandwidth products. The simulation results were compared with those obtained when investigating flow phantoms, both in attenuating and non-attenuating media. Moreover, in-vivo experiments are shown, demonstrating the improved penetration depth achievable in clinical settings.

The paper is organized as follows. After a short introduction on the pulse compression technique (Sec. II), section III reports on the ULA-OP implementation of the real-time Doppler imaging algorithm. Simulation and experimental settings, as well as the

Manuscript received February 3, 2016. This work was supported by the Italian Ministry of Education, University and Research (PRIN 2010-2011) and by the Wellcome Trust IEH Award [102431].

A. Ramalli, E. Boni, A. Dallai, F. Guidi, S. Ricci, P. Tortoli are with Department of Information Engineering, University of Florence, Firenze, Italy (e-mail: alessandro.ramalli@unifi.it).

adopted performance metrics, are described. Section IV compares the simulation results with those obtained in phantom experiments and presents in-vivo examples of application. The results are discussed in section V while concluding remarks are given in section VI.

II. Pulse Compression Basics

Fig. 1 shows an example of typical signals and spectra involved in a pulse compression system. The coded transmitted (TX) signal is defined as

$$s_{TX}(t) = a(t) \cdot \sin\left(2\pi f_0 t + \pi \frac{B}{T} t^2\right) \quad (1)$$

where T is the chirp length, t is the time ($t \in [-T/2\,;T/2]$), f_0 the chirp central frequency, B the spanned band and $a(t)$ is the tapering window. The compressed pulse $c(t)$ is obtained by convolving the received (RX) echo-signal with the matched filter $h(t)$:

$$h(t) = s_{TX}(-t) \quad (2)$$

Let's define B_{TX} as the −6dB effective bandwidth of the TX signal, which differs from B due to the effect of tapering. B_{TX} also corresponds to the ideal RX noise bandwidth. Considering a white noise distribution over the bandwidth B_{TX}, the transmission of chirp signals, compared to the transmission of standard sine bursts, can provide an SNR gain:

$$GSNR = 10\log_{10}(B_{TX}T) \quad (3)$$

Equation (3) is derived, in [26], according to the classic approach used in radar compression systems [27], where the *GSNR* is used to compare the received amplitudes when the same TX amplitude is used for both chirps and sine-bursts. Note that each doubling of B_{TX} yields a reduction of the SNR by about 6dB for sine-bursts and by 3dB for chirps. In both cases, in fact, the noise bandwidth increases, giving 3dB more noise power. However, the B_{TX} of sine-bursts is increased by reducing their length, which yields a 3dB reduction of the transmitted energy. Conversely, for linear chirps the transmitted energy, being related only to T, is not changed.

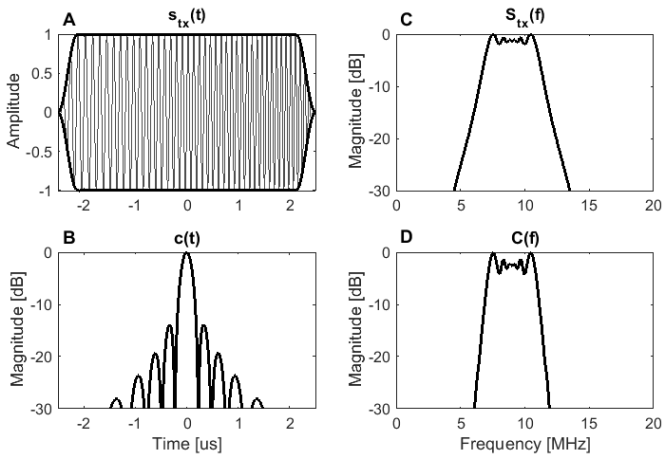

Fig. 1. Example of the main waveforms and spectra involved in a pulse compression system. A) typical shape of TX signal and matched filter impulse response; B) compressed pulse. C) and D) report the spectra corresponding to A) and B) , respectively.

III. Materials and Methods

A. ULA-OP real-time operation

The TX signal $s_{TX}(t)$ may be designed through a graphical application developed in Matlab® (Mathworks, Natick, MA, USA). The samples of $s_{TX}(t)$ feed the real-time software in a host PC, which sets the parameters (focus, aperture length, apodization, region of interest, etc) of the ultrasound acquisition. The software also replicates the $s_{TX}(t)$ signal for all of the active TX channels, and applies suitable delays and apodization coefficients according to the desired settings. A delta-sigma modulator, implemented in the software, converts the samples to bit-streams, one for each active TX channel. These bit-streams are then transferred to the ULA-OP memory. The software also computes 1024 coefficients of the base-band compressor spectrum $H_{bb}(f)$, which are transferred to the DSP (TMS320C6455, Texas Instruments, USA) on board ULA-OP [28].

Once ULA-OP is properly configured, the acquisition can start. In transmission, for each pulse repetition interval and each active element, the system field programmable gate arrays (FPGAs) read out the stored bit-streams at 600 Mb/s. By low-pass filtering such bit-streams the arbitrary waveform generator functionality is obtained. The generated signals are amplified by linear power amplifiers and channeled to the probe elements through a programmable 64 to 192 switch matrix. In reception, the weak echo-signals are channeled back to the system through the switch matrix, amplified by low noise programmable gain amplifiers, and sampled at 50 MSPS by 12-bit analog to digital converters. Four front-end FPGAs dynamically beamform the echoes by delaying, weighting and summing the RX samples. A fifth FPGA coherently demodulates the beamformed signal, applies a low-pass filter and down-samples the base-band components.

As shown in Fig. 2, the DSP transforms 512 quadrature (fast-time) samples through a 1024-point Fast Fourier Transform (FFT). The results are multiplied by the coefficients

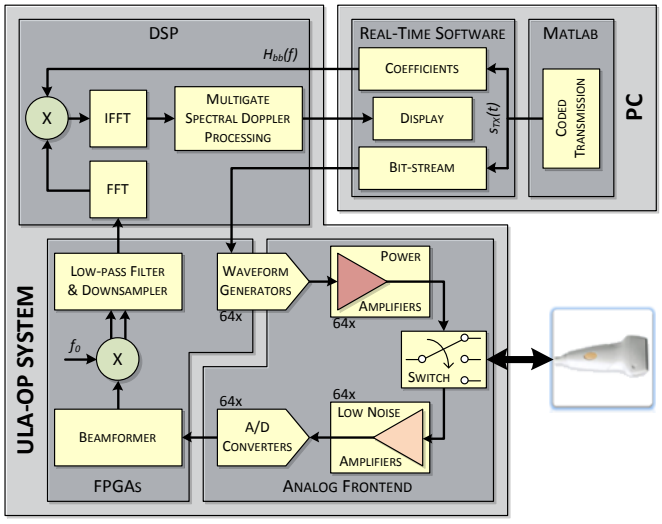

Fig. 2. Block-diagram of the system implemented for real-time pulse compression spectral Doppler experiments.

of the compression filter $H_{bb}(f)$, which is already initialized in the DSP memory. After the complex multiplications, the DSP transforms the spectral data back to the time domain through an Inverse FFT and selects 512 valid output samples, thus completing the pulse compression operation. The whole process is time critical and the DSP has to manage a large amount of data in real-time. For this reason, the code was hand-optimized by massive use of specific DSP functionalities (opcodes) that execute multiple operations in a single instruction, still maintaining 32-bit fixed point precision to maximize accuracy.

The DSP also produces real-time Doppler spectra related to one or multiple sample volumes corresponding to the 512 available depths. For each examined sample volume, one 128-point FFT is computed on a corresponding set of slow-time complex samples, which is obtained through a data reordering operation called corner-turning. Such operation is not feasible inside the (limited) internal memory of the processor. It was thus based on the external memories connected to the DSP, by exploiting the direct memory access coprocessor. The latter one lowers the workload of the main processor by storing the fast-time (pulse compressed) samples in a circular buffer, and then retrieving the same samples in a slow-time order prior to the spectral analysis.

The modules of the resulting spectra are thresholded to reduce noise, and displayed as spectrograms. When the spectral analysis is extended to multiple sample volumes, e.g. 512, an MSD frame is generated [24], and displayed by the host PC in a 512×128 pixel color-map. As shown in Fig. 3, in the MSD images the vertical axis corresponds to depth, while the horizontal axis reports the Doppler frequencies. These span a pulse repetition frequency (PRF) range, and can be arbitrarily shifted by the operator. Moreover, the elaborated samples can be stored in dynamic memories and downloaded on the PC for evaluation or additional post-processing, without interfering with the subsequent operations.

In order to evaluate the achievable performance, linear frequency modulated chirps of 2.5 and 5.0 μs length (including 10% tapering with a Tukey window), were generated. For each chirp signal duration, nine different bandwidths (B_{TX}) were tested, for a total of 18 experiments, as detailed in **Errore. L'origine riferimento non è stata trovata.**. In addition, 9 sine-bursts were considered, each having a different number of cycles and weighted by a proper Hamming window. The sine-burst lengths were tailored to obtain the same B_{TX} of the corresponding chirp signals (see **Errore. L'origine riferimento non è stata trovata.**). For all of the signals, both chirps and sine-bursts, the central frequency was 7 MHz.

B. Simulations

A numeric phantom was developed to simulate the flow in a wall-less cylindrical pipe with 8 mm diameter (Ø). The length of the pipe was 50 mm and it was centered at the TX focal depth, i.e. 25 mm. The scattering particles, simulated as point scatterers, moved according to a parabolic profile in steady laminar flow. The scatterers had a density of 40/mm^3 and their positions were updated every pulse repetition interval according to their velocity. The peak flow speeds was set to 80 cm/s and the flow was simulated over a 500 ms time interval at PRF=4 kHz, thus resulting in 2000 consecutive scatterer steps. The pipe was rotated to produce a Doppler angle of 70° that guarantees, for all of the simulated TX signals, the short sample volume condition. This states: "*the sample volume length (SVL) is sufficiently short and the Doppler angle sufficiently small, then the transmit time is determined by the SVL rather than the ultrasound beam width*" [29]. Therefore, the spectral broadening due to transit time depends on the transmitted bandwidth and not on the ultrasound beam width. For the propagation medium, two different attenuation coefficients (A_{tt}) were simulated, i.e. 0 and 0.5 dB/cm/MHz, corresponding to water and human tissue, respectively.

TABLE I. TRANSMITTED SIGNAL CHARACTERISTICS

Linear FM Chirps			B_{TX} [MHz]	Sine-Bursts	
***B* [MHz]**	***T* [μs]**	***Tapering***		***Weighting***	***Number of Cycles***
2	2.5 and 5	10% Tukey	**1.6**	Hamming	8.0
2.5			**2.2**		6.0
3			**2.7**		5.0
3.5			**3.2**		4.0
4			**3.6**		3.5
4.5			**4**		3.3
5			**4.5**		2.8
5.5			**5**		2.6
6			**5.4**		2.4

C. Phantom experiments

Two different flow phantoms were used. The first was constituted by a cylindrical tube (8 mm inner diameter and 1 mm thick wall) immersed in a water tank [30]. The tube was made by Rilsan®, a plastic material characterized by a sound velocity of 2600 m/s and attenuation of about 2 dB/cm/MHz. This phantom was used to test the performance of Doppler pulse compression in condition of negligible medium attenuation. The second phantom was the ATS524 (ATS Laboratories, Inc. Bridgeport, CT, USA), based on a tissue mimicking urethane rubber with attenuation coefficient of 0.5 dB/cm/MHz and speed of sound of 1450 m/s. This phantom includes one wall-less flow channel having Ø=8 mm. A wedge of the same tissue mimicking material was placed on the scanning surface to set the beam-to-flow angle at 70°.

A programmable peristaltic pump (Watson-Marlow, Falmouth, UK) pushed a blood-mimicking fluid in a homemade hydraulic circuit that could include any of the two phantoms. The blood-mimicking fluid consisted in 2.5 g of 10 μm polyamide spherical particles (Orgasol, Arkema Inc., Philadelphia, PA) suspended in 2 dm^3 of demineralized water [31]. 1 g of surface-active agent was added to obtain uniform particle distribution. The fluid flowed from a reservoir into an expansion tank, then through a 70 cm straight tube followed by the phantom and finally back to the reservoir. Here, the suspension was continuously stirred for at least 12 hours before the beginning of the experiments. The tested flow speed was 11.9 cm/s, corresponding to 180 ml/min. In these conditions the Reynolds number was low enough to ensure parabolic laminar

flow.

ULA-OP, connected to the LA533 linear array probe (Esaote SpA, Florence, Italy), was used to investigate the flow in the aforementioned phantoms. The same (linear chirp and sine-burst) Doppler pulses used in simulations were also employed in the experiments. The TX amplitude was set to 10 V, which is close to the maximum value (12.5 V) compatible with the linear transmitters onboard the ULA-OP and ensures limited non-linearity caused by near rail compression of the power amplifier. ULA-OP was programmed to interleave, at a machine PRF of 1500 Hz, the transmission of B-mode and Doppler pulses so that the Doppler PRF was 750 Hz. B-Mode was used to facilitate the probe positioning, while real-time spectrograms and MSD images produced by chirp or standard pulses were used to monitor the acquisition. Experimental demodulated data, with and without pulse compression - depending on the used TX signal - were saved to allow off-line processing.

D. *In-vivo experiments*

In the *in-vivo* tests, the ULA-OP was programmed to interleave the transmission of one pulse for B-mode imaging and two consecutive pulses for Doppler investigation along the same scan line. The first Doppler pulse was a 4-cycle sine burst (B_{TX}=3.2 MHz) while the second one was a 5µs-long linear chirp having the same B_{TX} of the sine burst (see **Errore. L'origine riferimento non è stata trovata.**). The TX amplitude of both Doppler pulses was 10 V. The machine PRF was set to 10 kHz, so that the Doppler PRF was 3.3 kHz for both transmitted pulses. The B-mode image, the two MSD frames and the related sonograms were simultaneously displayed in real-time. The threshold and the dynamics of each MSD frame and sonogram were set at the same values to permit a visual qualitative comparison of the performance. The common carotid artery and the carotid artery bifurcation of a healthy volunteer were examined by an experienced sonographer. During the exam, the interface of the real-time software was captured and a video file was saved.

E. *Data processing*

The MSD processing implemented in real-time in ULA-OP was replicated in Matlab in order to estimate the attained performance. The (simulated or experimental) down-sampled baseband data obtained after the transmission of sine-bursts or linear chirps were offline-processed. The related MSD frames were further averaged to produce smooth images, like that in Fig. 3. Here, S_{ROI} was defined as the region enclosed within the −6dB isolines and N_{ROI} was selected in the upper portion of the image, covering 40 gates, where the flow was absent (noise region). The SNR was thus estimated as:

$$SNR = 10\log_{10}\left(\frac{S}{N}\cdot\frac{n_N}{n_S}\right) \qquad (4)$$

where S and N correspond to the total power in S_{ROI} and N_{ROI}, and n_S and n_N and are the number of Doppler spectra (depths) involved in S_{ROI} and N_{ROI}, respectively. In our case, n_N is equal to 40, while n_S depends on the TX length [24].

Finally, the width of the profile in correspondence of the near wall (see Fig. 3) was assumed as an index of the axial resolution. As shown in [24], this width is in fact directly proportional to the sample volume length, which depends on the axial resolution.

IV. Results

A. *SNR measurements*

Fig. 4 shows the SNRs obtained from simulations and experiments for the sine-burst, short and long chirp signals listed in **Errore. L'origine riferimento non è stata trovata.**. The slope of each best fitting line is reported on the right. For each B_{TX}, the GSNR corresponds to the difference between the SNR values obtained for chirp and sine-burst transmissions, respectively.

In the simulations without tissue attenuation (Fig. 4A), the slopes of the best fitting lines are −5.9dB per octave for sine-bursts and of about −3dB per octave for linear chirps. Similar slopes (−6.4dB per octave for sine-bursts and of about −3.4/−3.5dB per octave for linear chirps), were obtained from the experiments (Fig. 4C). All of these slopes are very close to the expected −3dB and −6dB values.

The simulation and experimental GSNR values, which are also reported in TABLE II (columns A and C), are in general close to the values expected from (3). The simulation results, in particular, are higher - by up to 2.4dB for the longer chirps and up to 1.5dB for the shorter ones - than the expected ones.

Tissue attenuation (Fig. 4B and Fig.4D) does not significantly change the GSNR, since the differences with the values obtained for non-attenuating media are within 1.1 dB. However, the SNR best fit lines tend to even out, i.e. the SNR tend to decrease less than in no attenuating media. In simulations, the slopes of the best fit lines are −5.3dB per octave for sine-bursts and about −2.2/−1.9dB per octave for linear chirps, see Fig. 4B. The slope differences between simulations and experiments based on the ATS flow phantom (Fig. 4D) are within about ±0.5dB per octave. By comparing the results

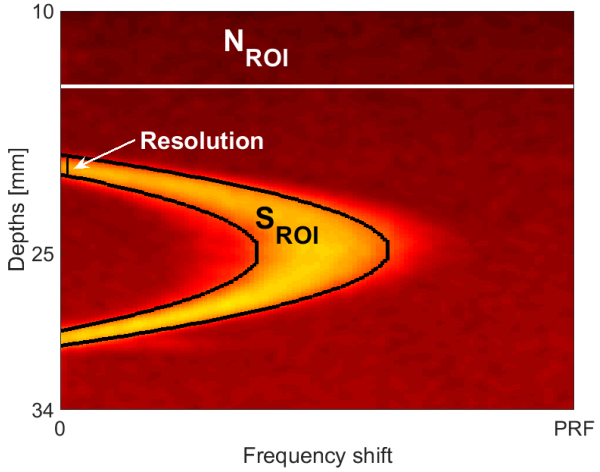

Fig. 3. Example of averaged multigate spectral Doppler image used to evaluate the pulse compression performance. Power spectral densities are coded to colors of increasing brightness. The data inside the signal (S_{ROI}) and noise (N_{ROI}) regions were used to evaluate the SNR.

obtained at 2.5 μs and 5 μs chirp lengths, the simulations confirm the expected 3dB difference while the experiments show a lower difference (around 2.3 dB) for both attenuating and non-attenuating media.

B. Resolution measurements

Fig. 5 reports the resolution values measured at different B_{TX}. In particular, since all of the values obtained for sine-bursts and chirps of equal bandwidth resulted very close, they were averaged. In general, the resolution improves with bandwidth, as expected. However, when the frequency dependent attenuation is considered (red dotted line), for signals with B_{TX}≥4 MHz, the resolution tends to flatten.

In the experiments (Fig. 5 bottom), in particular, the values are 10 to 25 μm worse than those measured in simulations (Fig. 5 top). This small difference (≈10%) may be attributed to the clutter, which was not included in the simulations.

C. Thermal and mechanical indexes

Since long coded signals involve increased energy transfer to the human body, both the thermal index (TI) and the mechanical index (MI) were experimentally estimated according to NEMA standards [32], [33] to ensure the safety of the ultrasound system. In particular, the thermal index model that best fits our

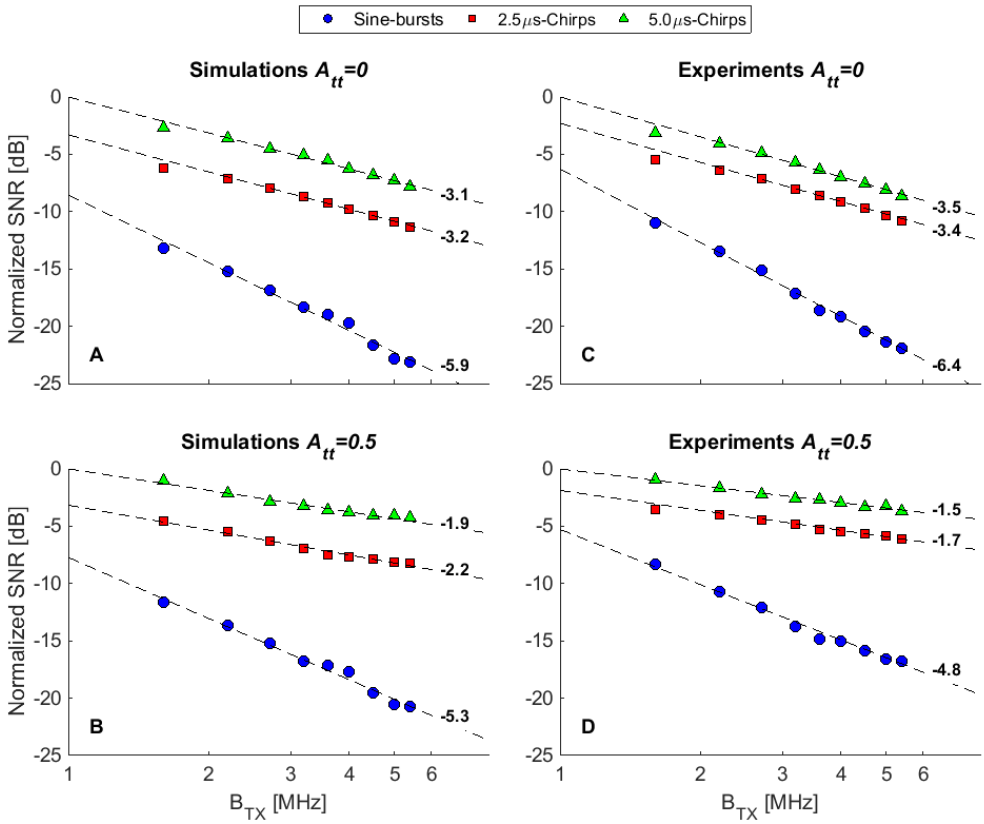

Fig. 4. Effect of transmitted bandwidth B_{TX} on the SNR for sine-burst and chirp transmission in simulations (A, B) and experiments (C, D). Upper panels (A, C) were obtained for propagation in water, while lower panels (B, D) were obtained for a medium with 0.5 dB/cm/MHz attenuation coefficient. The numbers on the bottom right of each trend line are expressed in dB per octave.

TABLE II. EXPECTED VS ESTIMATED GSNR IN SIMULATIONS AND ACQUISITIONS RELATED TO THE RESULTS SHOWN IN FIG. 4.

	***Expected* GSNR [dB]**		***Estimated* GSNR [dB]**							
			Simulations				***Experiments***			
B_{TX} [MHz]	*T=2.5 μs*	*T=5 μs*	***A*** A_{tt} =0		***B*** A_{tt} =0.5		***C*** A_{tt} =0		***D*** A_{tt} =0.5	
			T=2.5 μs	*T=5 μs*	*T=2.5 μs*	*T=5 μs*	*T=2.5 μs*	*T=5 μs*	*T=2.5 μs*	*T=5 μs*
1.6	6.0	9.0	7.1	10.6	7.0	10.5	5.1	7.4	5.5	7.7
2.2	7.4	10.4	8.1	11.6	8.0	11.5	6.9	9.1	7.1	9.3
2.7	8.3	11.3	9.0	12.4	8.9	12.3	7.7	10.0	8.0	10.1
3.2	9.0	12.0	9.8	13.5	9.7	13.2	8.8	11.1	9.1	11.4
3.6	9.5	12.6	9.7	13.6	9.6	13.3	9.5	12.0	10.0	12.1
4	10.0	13.0	10.1	13.8	9.9	13.4	9.6	12.0	9.9	12.0
4.5	10.5	13.5	11.7	15.4	11.4	14.8	10.0	12.4	10.7	12.8
5	11.0	14.0	12.5	16.4	12.0	15.6	10.5	13.1	11.0	13.2
5.4	11.3	14.3	12.7	16.5	11.8	15.4	10.6	13.1	11.1	13.3

application is the one for soft tissue, small apertures (<1 cm^2) and unscanned modes. The MI and TI were measured for all of the signals reported in **Errore. L'origine riferimento non è stata trovata.** with 10V transmit amplitude. The TI, in particular, was estimated at the same Doppler PRF (3.3 kHz) used for in-vivo tests (see section III.D). The MI was 0.31±0.04. The TI turned out to be 0.07±0.02, 0.35±0.02, and 0.67±0.05 for sine-bursts, 2.5 µs and 5 µs long chirps, respectively.

D. In-vivo experiments

Fig. 6, showing a screenshot extracted from the linked (Clip1.avi), illustrates the ULA-OP real-time interface used during the in-vivo scan of the common carotid artery of a healthy volunteer. This example allows comparing the spectrogram and MSD images simultaneously obtained by the transmission of 4-cycle sine-bursts (Fig. 6B-D) and of 5µs-long linear chirp, both having B_{TX}=3.2 MHz (Fig. 6C-E). In both cases, the transmission amplitude was set to 10 V, thus yielding MI=0.30 and TI=0.07 for the sine-burst and MI=0.33 and TI=0.69 for the chirp.

The spectrograms from the vessel center (Fig. 6D-E) were detected for both transmit signals, but the SNR obtained by pulse compression is clearly improved. The same SNR gain, which was here estimated to be 10dB is evident from the MSD images (Fig. 6B-C). Such images, in particular, highlight the characteristic M-shape profile [34], [35] detected at late systole.

Fig. 7 shows one frame extracted from the linked clip (Clip2.avi), related to the exam of the right carotid bifurcation of a healthy volunteer (Fig. 7A). The spectra in Fig. 7B-D prove that the SNR obtained with the sine-burst TX was not sufficient to examine the deeper vessels. Indeed the fat layers attenuated too much the weak echo signals obtained by keeping the TX level at 10V amplitude. Only the velocity profile from the superior thyroid artery is barely visible in Fig. 7B. On the contrary, the spectra in Fig. 7C-E were clearly detected and the profile shapes of the external and internal carotid are well defined. In Fig. 7E, the spectrogram emerging from noise thanks to the pulse compression algorithm highlights the flow complexity in correspondence of the inner carotid artery close to the bifurcation.

V. Discussion

In this paper, the real-time pulse compression method applied to beamformed, demodulated and down-sampled echo-data, developed in [36] for imaging purposes, was modified to fit (multigate) spectral Doppler applications. The DSP procedure, in particular, was optimized to make possible at high speed the corner turning operation (from fast- to slow-time) involved in multigate Doppler operation. Furthermore, a thorough investigation of the performance, in terms of SNR and axial resolution, achievable for different TX bandwidths has been reported. Simulations were carried out to obtain a reference for the evaluation of the experimental results. The results demonstrate that chirp excitation and pulse compression is feasible, in real-time, in a low-cost scanner using a single DSP and linear transmitters with limited TX voltage.

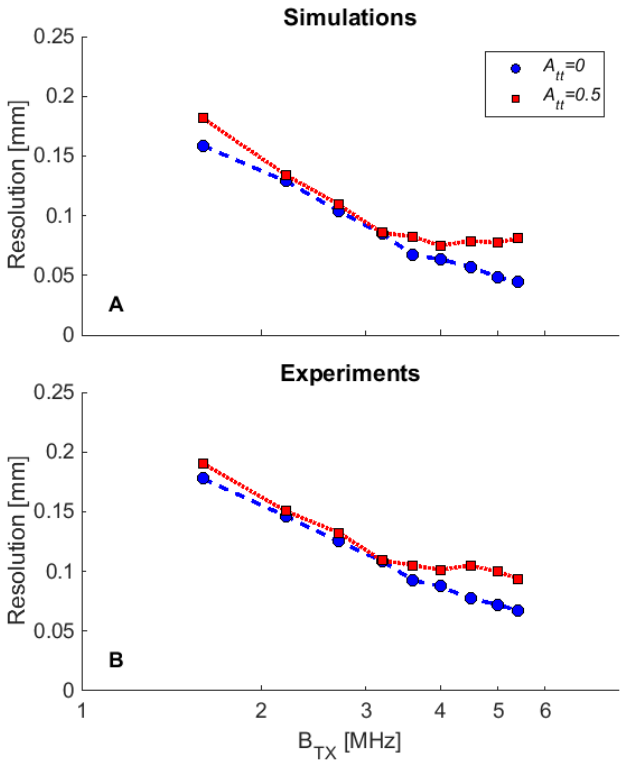

Fig. 5. Effect of transmitted bandwidth on the axial resolution evaluated from the MSD data. The values obtained for the different signals having the same B_{TX} were averaged. Simulated (top) and experimental (bottom) values obtained for a parabolic velocity profile and attenuating (red dotted line) or non attenuating (blue dashed line) medium.

Both simulations and experiments confirmed that in non-attenuating media, by doubling the TX bandwidth the SNR degrades by about 3 and 6 dB for chirp and sine burst, respectively. In particular, the simulated GSNRs turn out to be higher (by 1.5-2.4 dB) than the values expected from (3). Such differences can be explained by considering that the sine-burst spectrum is not flat across the whole bandwidth, as it is supposed to be in the derivation of (3) [26], while it is indeed nearly flat for linear chirps, especially for the longer ones.

Similar trends were obtained when the selective attenuation was considered. The simulations, in particular, highlight that, over the spanned bandwidth, the GSNR is reduced by less than 1.1dB. This reduction can be explained by considering that the wider is the chirp bandwidth the more the selective attenuation distorts the spectrum of the received echo-signal [25], [36].

For both attenuating and non-attenuating media, the experimental results outline that by doubling the chirp duration (from 2.5 µs to 5 µs) the SNR increases less than expected (2.3dB vs 3dB). This small (0.7dB) difference can be attributed to the multiple sources of non-ideality that typically affect the experimental measurements.

In terms of axial resolution (Fig. 5), chirps and sine-bursts perform similarly with and without attenuation. For bandwidths wider than 4 MHz, the frequency dependent attenuation filters the RX signals so that the effective bandwidth is reduced [36], with a consequent loss of resolution highlighted by the flat regions in Fig. 5.

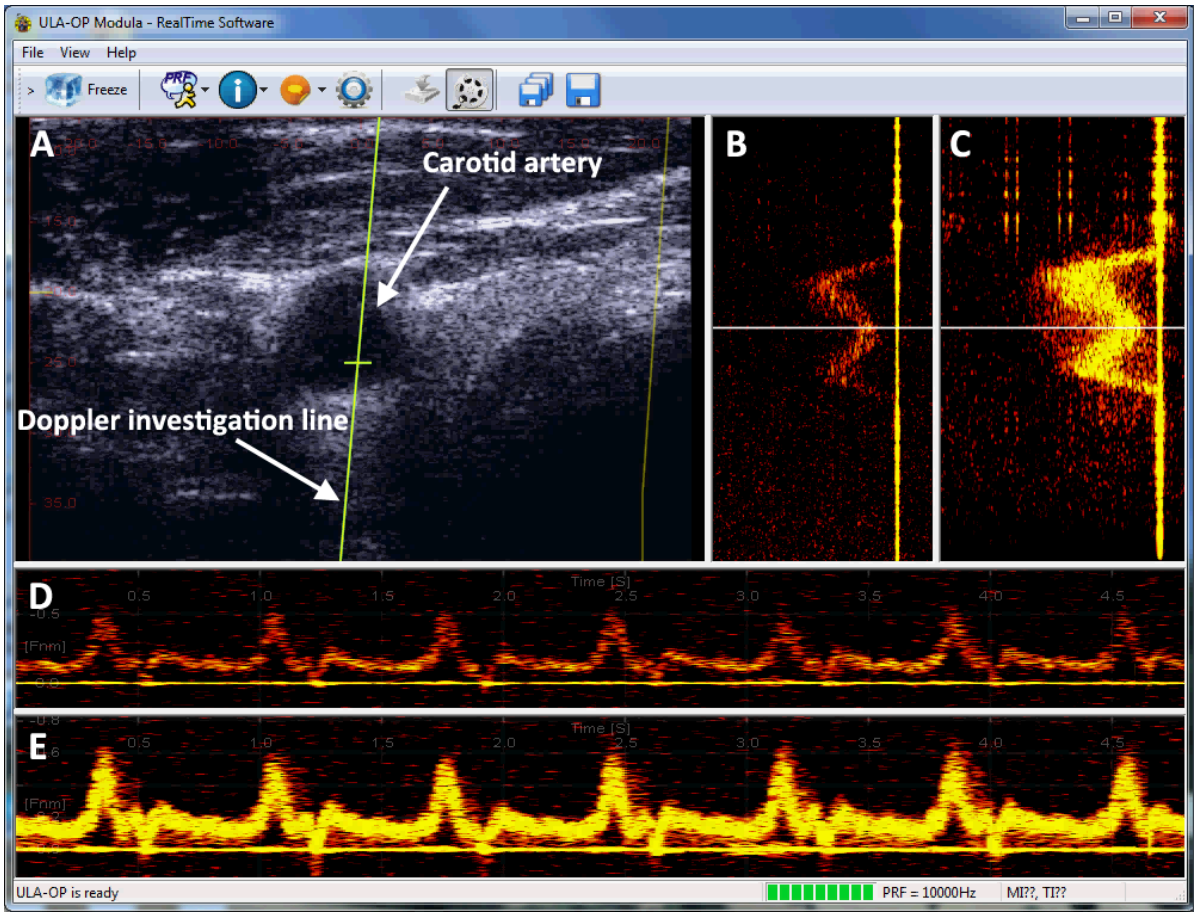

Fig. 6. ULA-OP real-time display when the carotid artery of a healthy volunteer was examined. The frame was extracted from the linked clip (Clip1.avi) and was freezed during the late systole. (A) B-mode image: the yellow line highlights the Doppler investigation line. Multigate spectral Doppler images obtained by transmitting a 4-cycle sine burst (B) and a 5μs-long linear chirp with B=3.5 MHz (C), both at 10 V transmission amplitude and 7 MHz center frequency. Spectrograms (D-E) related to the depth selected through the white cursor in B and C, respectively. The depth range was here 8-37 mm.

Since all above results could be, in principle, influenced by the chosen parabolic profile shape, which could lead to loss of performance due to velocity broadening within a same sample volume, we repeated simulations and experiments also for a parabolic profile with a 40% lower peak velocity. Moreover, simulations were repeated also for two flat profiles with the same velocities. However, the SNR results turned out to be equivalent to those reported above, with a deviation limited to ±0.2dB. These results were thus not reported for brevity and to improve the readability of figures and tables.

The results confirm the tradeoff among bandwidth, axial resolution and SNR: the wider the bandwidth, the better is the resolution, and the lower is the SNR. This is valid also for chirp signals, even though the SNR gain increases with bandwidth (see Fig. 4). Hence, in each application, the highest possible SNR value is obtained by pulse compression with bandwidth limited to the minimum acceptable value that grants the desired resolution. Increasing the TX duration may be beneficial for the SNR, but not as much as predicted. In addition, considering that longer TX signals also yield higher TIs, it looks reasonable limiting the maximum TX duration to the values used in this work, which provided significant SNR improvements.

A known drawback of pulse compression techniques consists in the so-called range-lobes that introduce image artifacts. They are detrimental for B-mode imaging and can be dampened by the so-called mismatched filter technique [26]. However, in pulsed wave spectral Doppler systems, the involved dynamics is typically low (<20dB), because of the weak scattering of red blood cells. Therefore, the level of range-lobes tends to be under the noise level and does not significantly affect the resulting spectra, as shown in Fig. 6 and Fig. 7.

The in-vivo tests proved that, although the time-bandwidth products of the used chirp signal were relatively low, a significant gain (10 dB) was actually obtained. Fig. 6 shows that the resolution and spectral broadening obtained with sine bursts and chirps are qualitatively comparable, while the SNR, and thus the penetration depth, was clearly improved by chirp transmission. Typically, the commercial scanners increase the penetration depth by increasing either the pulse length (with worsen resolution) or the transmission amplitude up to the levels permitted by MI and TI limitations. The transmission amplitudes (e.g. 10 V) set in our experimental tests, stay within the maximum value (12.5 V) compatible with ULA-OP arbitrary waveform generators, and are surely lower than those permitted by most scanners. However, to reliably measure the achievable SNR gain, the same amplitude for the TX signals to be compared had to be used. Our results also allow estimating, for example, how much the amplitude of the sine bursts should

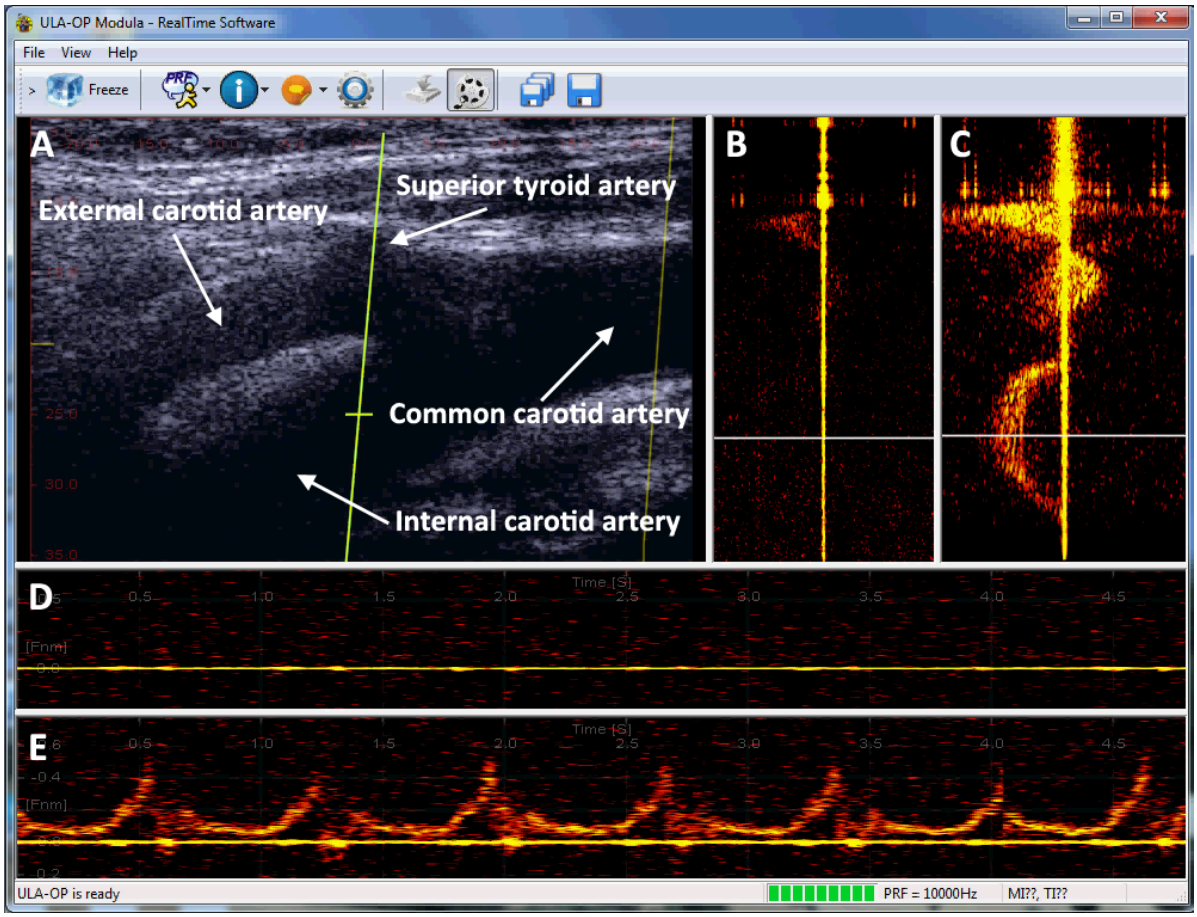

Fig. 7. ULA-OP real-time display when the right bifurcation of the internal carotid artery, the external carotid artery and the superior tyroid artery of a healthy volunteer were examined. The frame was extracted from the linked clip (Clip2.avi) and was freezed during the systole peak. (A) B-mode image: the yellow line highlights the Doppler investigation line. Multigate spectral Doppler images obtained by transmitting a 4-cycle sine burst (B) and a 5μs-long linear chirp with B=3.5 MHz (C), both at 10 V transmission amplitude and 7 MHz center frequency. Spectrograms (D-E) related to the depth selected through the white cursor in B and C, respectively. The depth range was 5-35 mm.

be increased to produce an equivalent SNR. A 10dB SNR improvement would be obtained by raising the TX amplitude to 32 V (with a corresponding MI in the order of 0.9), which is actually close to the limit frequently imposed by the software of commercial scanners for the transmission of 4-cycle bursts. Chirp-based coding at low TX levels allows maintaining high spatial resolution while improving the sensitivity without compromising the safety of the ultrasound system. Indeed, the measured MIs and TIs resulted well below the limits suggested in [37], up to the point that it would not be required to reduce the exposure time in non-obstetric and non-neonatal ultrasound applications.

The SNR gain provided by pulse compression might improve the detection of flow in cardiac and transcranial applications, or in difficult subjects [18] in particular at low TX voltage levels. In high-quality state-of-the-art ultrasound systems pulse compression could be used to increase the transmission frequency, and thus the spatial resolution, while maintaining adequate penetration depth. On the other hand, the gain achievable with pulse compression could be beneficial in color Doppler applications (as already demonstrated in the Sequoia scanner), or to improve battery saving for battery supplied equipment such as mobile (based on tablets) or wireless systems. Indeed both linear and bipolar pulsers with lower peak voltages (e.g. 12 V) could be employed so as to avoid any loss in the DC/DC conversion from the battery supply to the high rail power supply.

VI. Conclusion

This paper has shown that the pulse compression technique may be suitably integrated in a low-cost scanner like ULA-OP, to be profitably used in spectral Doppler applications. By operating on beamformed, demodulated and down-sampled data in the frequency domain, a single DSP is sufficient to perform both pulse compression and (multigate) spectral Doppler algorithms. Both in-vitro and in-vivo experiments demonstrated that, compared to the transmission of typical sine-bursts, the transmission of short (5 μs) linear frequency modulated chirps and matched RX filtering may improve the SNR by more than 13 dB without loss of resolution.

Ackowledgment

The authors gratefully thank Dr. D. Righi (Heart and Vessels Department, AOU Careggi, Florence, Italy) for valuable help in performing in-vivo acquisitions.

REFERENCES

[1] M. H. Pedersen, T. X. Misaridis, and J. A. Jensen, "Clinical evaluation of chirp-coded excitation in medical ultrasound," *Ultrasound Med. Biol.*, vol. 29, no. 6, pp. 895–905, Jun. 2003.
[2] S. Harput, "Use of chirps in medical ultrasound imaging," PhD Thesis, University of Leeds, 2012.
[3] M. O'Donnell, "Coded excitation system for improving the penetration of real-time phased-array imaging systems," *IEEE Trans. Ultrason. Ferroelectr. Freq. Control*, vol. 39, no. 3, pp. 341 –351, May 1992.
[4] M. L. Oelze, "Bandwidth and resolution enhancement through pulse compression," *IEEE Trans. Ultrason. Ferroelectr. Freq. Control*, vol. 54, no. 4, pp. 768–781, 2007.
[5] M. Lewandowski and A. Nowicki, "High frequency coded imaging system with RF software signal processing," *IEEE Trans. Ultrason. Ferroelectr. Freq. Control*, vol. 55, no. 8, pp. 1878–1882, 2008.
[6] A. Polpetta and P. Banelli, "Design and performance of Huffman sequences in medical ultrasound coded excitation," *IEEE Trans. Ultrason. Ferroelectr. Freq. Control*, vol. 59, no. 4, pp. 630 –647, Apr. 2012.
[7] C. Yoon, W. Lee, J. Chang, T. Song, and Y. Yoo, "An efficient pulse compression method of chirp-coded excitation in medical ultrasound imaging," *IEEE Trans. Ultrason. Ferroelectr. Freq. Control*, vol. 60, no. 10, pp. 2225–2229, 2013.
[8] V. Behar and D. Adam, "Parameter optimization of pulse compression in ultrasound imaging systems with coded excitation," *Ultrasonics*, vol. 42, no. 10, pp. 1101–1109, Aug. 2004.
[9] T. Misaridis and J. A. Jensen, "Use of modulated excitation signals in medical ultrasound. Part II: design and performance for medical imaging applications," *IEEE Trans. Ultrason. Ferroelectr. Freq. Control*, vol. 52, no. 2, pp. 192–207, Feb. 2005.
[10] R. Y. Chiao and Xiaohui Hao, "Coded excitation for diagnostic ultrasound: a system developer's perspective," *IEEE Trans. Ultrason. Ferroelectr. Freq. Control*, vol. 52, no. 2, pp. 160–170, Feb. 2005.
[11] J. M. G. Borsboom, C. T. Chin, A. Bouakaz, M. Versluis, and N. de Jong, "Harmonic chirp imaging method for ultrasound contrast agent," *IEEE Trans. Ultrason. Ferroelectr. Freq. Control*, vol. 52, no. 2, pp. 241–249, Feb. 2005.
[12] J. R. Sanchez and M. L. Oelze, "An ultrasonic imaging speckle-suppression and contrast-enhancement technique by means of frequency compounding and coded excitation," *IEEE Trans. Ultrason. Ferroelectr. Freq. Control*, vol. 56, no. 7, pp. 1327–1339, Jul. 2009.
[13] J. Song, S. Kim, H. Sohn, T. Song, and Y. M. Yoo, "Coded excitation for ultrasound tissue harmonic imaging," *Ultrasonics*, vol. 50, no. 6, pp. 613–619, May 2010.
[14] S. Harput, J. McLaughlan, D. M. J. Cowell, and S. Freear, "Superharmonic imaging with chirp coded excitation: filtering spectrally overlapped harmonics," *IEEE Trans. Ultrason. Ferroelectr. Freq. Control*, vol. 61, no. 11, pp. 1802–1814, Nov. 2014.
[15] J. Liu and M. F. Insana, "Coded Pulse Excitation for Ultrasonic Strain Imaging," *IEEE Trans. Ultrason. Ferroelectr. Freq. Control*, vol. 52, no. 2, pp. 231–240, Feb. 2005.
[16] H. Peng and D. C. Liu, "Chirp-Coded Pulse Excitation for Ultrasound Elasticity Imaging," in *2010 4th International Conference on Bioinformatics and Biomedical Engineering (iCBBE)*, 2010, pp. 1–4.
[17] P. Song, M. W. Urban, A. Manduca, J. F. Greenleaf, and S. Chen, "Coded excitation plane wave imaging for shear wave motion detection," *IEEE Trans. Ultrason. Ferroelectr. Freq. Control*, vol. 62, no. 7, pp. 1356–1372, Jul. 2015.
[18] R. S. Finkelhor, M. Moallem, and R. C. Bahler, "Characteristics and Impact of Obesity on the Outpatient Echocardiography Laboratory," *Am. J. Cardiol.*, vol. 97, no. 7, pp. 1082–1084, Apr. 2006.
[19] R. Y. Chiao, L. Y. Mo, A. L. Hall, S. C. Miller, and K. E. Thomenius, "B-mode blood flow (B-flow) imaging," in *2000 IEEE Ultrasonics Symposium*, 2000, vol. 2, pp. 1469–1472 vol.2.
[20] J. K. Tsou, J. Liu, and M. F. Insana, "Modeling and phantom studies of ultrasonic wall shear rate measurements using coded pulse excitation," *IEEE Trans. Ultrason. Ferroelectr. Freq. Control*, vol. 53, no. 4, pp. 724–734, Apr. 2006.
[21] J. Cowe, J. Gittins, and D. H. Evans, "Improving Performance of Pulse Compression in a Doppler Ultrasound System Using Amplitude Modulated Chirps and Wiener Filtering," *Ultrasound Med. Biol.*, vol. 34, no. 2, pp. 326–333, Feb. 2008.
[22] B. Lamboul, "Analysis of the potential for coded excitation to improve the detection of tissue and blood motion in medical ultrasound.," PhD Thesis, University of Edinburgh, 2010.
[23] E. Boni, L. Bassi, A. Dallai, F. Guidi, A. Ramalli, S. Ricci, R. J. Housden, and P. Tortoli, "A reconfigurable and programmable FPGA-based system for nonstandard ultrasound methods," *IEEE Trans. Ultrason. Ferroelectr. Freq. Control*, vol. 59, no. 7, pp. 1378 –1385, Jul. 2012.
[24] P. Tortoli, F. Guidi, G. Guidi, and C. Atzeni, "Spectral velocity profiles for detailed ultrasound flow analysis," *IEEE Trans. Ultrason. Ferroelectr. Freq. Control*, vol. 43, no. 4, pp. 654–659, Jul. 1996.
[25] A. Ramalli, A. Dallai, E. Boni, F. Guidi, S. Ricci, and P. Tortoli, "Real-time pulse compression in multigate spectral Doppler imaging," in *Ultrasonics Symposium (IUS), 2015 IEEE International*, 2015.
[26] T. Misaridis and J. A. Jensen, "Use of modulated excitation signals in medical ultrasound. Part I: basic concepts and expected benefits," *IEEE Trans. Ultrason. Ferroelectr. Freq. Control*, vol. 52, no. 2, pp. 177–191, Feb. 2005.
[27] J. R. Klauder, A. C. Price, S. Darlington, and W. J. Albersheim, "The theory and design of chirp radars," *Bell Syst. Tech. J.*, vol. 39, no. 4, pp. 745–808, Jul. 1960.
[28] A. Ramalli, F. Guidi, E. Boni, and P. Tortoli, "Real-time base-band pulse compression imaging," in *International Ultrasonics Symposium (IUS), 2013 Proceedings, 2013 IEEE*, pp. 2002–2005.
[29] D. H. Evans and W. N. McDicken, *Doppler Ultrasound: Physics, Instrumentation and Signal Processing*, 2nd Edition. Wiley-Blackwell, 1999.
[30] M. Lenge, A. Ramalli, E. Boni, H. Liebgott, C. Cachard, and P. Tortoli, "High-frame-rate 2-D vector blood flow imaging in the frequency domain," *IEEE Trans. Ultrason. Ferroelectr. Freq. Control*, vol. 61, no. 9, pp. 1504–1514, Sep. 2014.
[31] K. V. Ramnarine, D. K. Nassiri, P. R. Hoskins, and J. Lubbers, "Validation of a New Blood-Mimicking Fluid for Use in Doppler Flow Test Objects," *Ultrasound Med. Biol.*, vol. 24, no. 3, pp. 451–459, Mar. 1998.
[32] American Institute of Ultrasound in Medicine, "Acoustic Output Measurement Standard for Diagnostic Ultrasound Equipment." National Electrical Manufacturers Association, 2004.
[33] American Institute of Ultrasound in Medicine, "Standard for Real-Time Display of Thermal and Mechanical Acoustic Output Indices on Diagnostic Ultrasound Equipment." National Electrical Manufacturers Association, 2004.
[34] P. Tortoli, V. Michelassi, G. Bambi, F. Guidi, and D. Righi, "Interaction between secondary velocities, flow pulsation and vessel morphology in the common carotid artery," *Ultrasound Med. Biol.*, vol. 29, no. 3, pp. 407–415, Mar. 2003.
[35] R. Krams, G. Bambi, F. Guidi, F. Helderman, A. F. W. van der Steen, and P. Tortoli, "Effect of vessel curvature on Doppler derived velocity profiles and fluid flow," *Ultrasound Med. Biol.*, vol. 31, no. 5, pp. 663–671, May 2005.
[36] A. Ramalli, F. Guidi, E. Boni, and P. Tortoli, "A real-time chirp-coded imaging system with tissue attenuation compensation," *Ultrasonics*, vol. 60, pp. 65–75, Jul. 2015.
[37] Safety Group of the British Medical Ultrasound Society, "Guidelines for the safe use of diagnostic ultrasound equipment," *Ultrasound*, vol. 18, no. 2, pp. 52–59, May 2010.

Alessandro Ramalli (M'10) was born in Prato, Italy, in 1983. In 2008, he graduated in Electronics engineering from the University of Florence. In 2012 he earned the PhD degree in Electronics System Engineering from the University of Florence and in Automatics, Systems and Images from the University of Lyon, by defending a thesis on the development of novel ultrasound techniques for imaging and elastography. Alessandro currently holds a postdoctoral position at the MSD Laboratory of the University of Florence, where he is involved in the development of the imaging section of a programmable open ultrasound system. His research interests include medical imaging, ultrasound simulation and elastography.

Enrico Boni was born in 1977 in Florence, Italy. He graduated in electronic engineering on 2001 at the University of Florence, Italy and received the PhD degree in Electronic System Engineering on 2005 from the University of Florence, Italy. He currently holds a Research position at the Microelectronic System Design Laboratory, Department of Information Engineering, University of Florence, Italy. His research interests include analog and digital system design, digital signal processing algorithm, digital control systems, Doppler ultrasound signal processing, microemboli detection and classification.

Alessandro Dallai was born in Florence, Italy, in 1979. His lively interest in electronics has prompted him to pursue the Laurea degree and the Ph.D. in electronic engineering, respectively received in 2004 and 2009 from the University of Florence. In 2005 he spent one year working with software-defined-radios for avionics. Currently, he is involved in multiple research programs in the department of Information Engineering at the University of Florence, mainly regarding the improvement of novel ultrasound systems, which in the past years contributed to the development of a worldwide appreciated platform for research on ultrasound. His academic interests focus on electronic system design and highly-optimized DSP firmware development.

Francesco Guidi was born in Portoferraio (LI), Italy, in 1964. He graduated from the University of Florence, Italy, with the M.Sc. degree in electronics engineering and subsequently he received his Ph.D. degree in electronic systems engineering. After working in a national company on the design of a real time radiologic image processing system, he joined the National Institute of Nuclear Physics (INFN) where he was involved in the design of real time software for solid state particle detectors. Since 1992, Francesco has held a position at the Electronics and Telecommunications Department of the University of Florence. His research interests include the development of real-time methods for ultrasound blood flow estimation and the investigation of acoustic properties of ultrasound contrast agents.

Stefano Ricci (M'07-SM'16) received the degree in Electronic Engineering in 1997, and the Ph.D. degree in Electronic Systems Engineering in 2001, both from the University of Florence. Since 2006 he works as researcher at the Electronics and Telecommunications Department (recently changed in Information Engineering Department) of the University of Florence. His research activities are focused on the development of high performance ultrasonic systems and the development and test of new ultrasound methods for medical and industrial applications. Stefano Ricci is author of more than 60 publications in international conferences and journals.

Piero Tortoli (M'91-SM'96) received the Laurea degree in electronics engineering from the University of Florence, Italy, in 1978. Since then, he has been on the faculty of the Electronics and Telecommunications (now Information Engineering) Department of the University of Florence, where he is currently full Professor of Electronics, leading a group of over 10 researchers in the Microelectronics Systems Design Laboratory.

Professor Tortoli has served on the IEEE International Ultrasonics Symposium Technical Program Committee since 1999 and is currently Associate Editor for the UFFC Transactions. He chaired the 22nd International Symposium on Acoustical Imaging (1995), the 12th New England Doppler Conference (2003) and established the Artimino Conference on Medical Ultrasound in 2011. In 2000, he was named an Honorary Member of the Polish Academy of Sciences. Professor Tortoli's research activity is centered on the development of ultrasound research systems and novel imaging/Doppler methods, on which he has published more than 200 papers.